JOURNAL OF THERMOPHYSICS AND HEAT TRANSFER
Vol. 23, No. 3, July–September 2009

Rotational-Temperature Measurements of Chemically Reacting CN Using Band-Tail Spectra

Kosuke Kurosawa* and Seiji Sugita†
University of Tokyo, Kashiwa, Chiba 277-8561, Japan
Kazuhisa Fujita‡
Japan Aerospace Exploration Agency, Chofu, Tokyo 229-8510, Japan
Ko Ishibashi§
University of Tokyo, Bunkyo-ku, Tokyo 113-0033, Japan
Toshihiko Kadono¶
Osaka University, Suita, Osaka 565-0871, Japan
Sohsuke Ohno**
Chiba Institute of Technology, Tsudanuma, Chiba 275-0016, Japan
and
Takafumi Matsui††
University of Tokyo, Kashiwa, Chiba 277-8561, Japan

DOI: 10.2514/1.40037

The vibrational state of chemically reacting CN radicals does not necessarily have a Boltzmann distribution because it may be influenced by the chemical reaction leading to the formation of the CN radicals. Here, we develop a new method to measure the rotational temperature of chemically reacting nonequilibrium cyanide radicals using the band tails of their emission spectra. Because of the very short relaxation time scales, both the translational and rotational states reach a thermal equilibrium even when the vibrational state does not have a Boltzmann distribution. The method proposed in this study has two advantages. First, it is not sensitively affected by self-absorption. Second, it does not require as high a wavelength resolution as other methods because it uses the overall shape of the tail part of the CN emission bands. Thus, our method is more suitable for high-speed temperature measurements, where a high-wavelength-resolution measurement is difficult to obtain. To investigate the validity of our method, we carried out laser-ablation experiments within an $N_2 - H_2O - CO_2 -$ Ar gas mixture using graphite targets and measured the rotational temperature of laser-induced CN and C_2 radicals using the proposed method. The rotational temperatures exhibit reasonable trends as functions of time and beam cross sections, strongly suggesting that our method is useful for translational–rotational-temperature estimation of chemically reacting nonequilibrium CN radicals.

Nomenclature

A = transition probability
c = light speed
Er = the square mean of the difference between the observed and theoretical synthetic spectra
F = rotational energy
h = Planck constant
I_{obs} = spectral irradiance of an observed spectrum
I_{syn} = spectral irradiance of a synthetic spectrum
I_{true} = spectral irradiance of a true spectrum
J' = rotational quantum number of an upper electron state
J'' = rotational quantum number of a lower electron state
k = Boltzmann constant
N = number density of an upper electron state
T_{rot} = translational–rotational temperature
T_{vib} = vibrational–electron–electronic temperature
ν' = vibrational quantum number of an upper electron state
ν'' = vibrational quantum number of a lower electron state
λ = wavelength
Ψ = irradiance of the instrument function of a spectrograph

Received 25 July 2008; accepted for publication 2 April 2009.

*Graduate Student, Department of Complexity Science and Engineering, 5-1-5, Kashiwanoha; kurosawa@astrobio.k.u-tokyo.ac.jp. Student Member AIAA.

†Associate Professor, Department of Complexity Science and Engineering, 5-1-5, Kashiwanoha; sugita@k.u-tokyo.ac.jp. Member AIAA.

‡Senior Researcher, Institute of Aerospace Technology, 7-44-1, Jindaiji Hhigashi-machi; kazudom@chofu.jaxa.jp. Senior Member AIAA.

§Graduate Student, Department of Earth and Planetary Science, 7-3-1, Hongo; ishibashi@impact.k.u-tokyo.ac.jp.

¶Associate Professor, Institute of Laser Engineering, 2-6, Yamadaoka; kadonot@ile.osaka-u.ac.jp.

**Postdoctoral Researcher, Planetary Exploration Center, 2-17-1, Narashino; sohsuke.ohno@it-chiba.ac.jp.

††Professor, Department of Complexity Science and Engineering, 5-1-5, Kashiwanoha; matsui@k.u-tokyo.ac.jp.

I. Introduction

TEMPERATURE is one of the most important thermodynamic quantities in shock-induced chemistry because it is a key parameter in chemical reactions. Emission spectroscopy is often used for temperature estimation of self-luminous high-temperature gas because it is nonintrusive [1]. In general, an emission spectrum from diatomic molecules exhibits a specific structure containing a large number of rotational lines in a narrow range of wavelengths, because diatomic molecules have internal degrees of freedom such as those allowed by vibration and rotation. Extremely high spectral resolution and a high signal-to-noise (S/N) ratio are required to separate individual rotational lines within a band spectrum. Thus, spectral-form-inversion analysis, which iteratively compares a theoretical synthetic spectrum and an observed spectrum for different controlling parameters, is widely used for temperature estimation of self-

luminous diatomic molecules [2–5]. The parameter set that minimizes the difference between the observed and theoretical spectra is considered the maximum-likelihood estimate (MLE) of the temperature of the observed high-temperature gas. This is a useful method in estimating the temperature of self-luminous diatomic molecules if each molecular state (e.g., translational, vibrational, rotational, electron translational, and electron excitation) has a Boltzmann distribution.

CN radicals are among the best molecules for temperature measurements of high-temperature gas because their emission efficiency is very high and because they are stable at high temperatures for a wide range of chemical compositions. In addition, CN is one of the most important molecules in shock-induced chemistry, including studies of the atmospheric entry of probe vehicles [6], the production of carbon-nitride thin films [3], and meteoritic impacts on Earth [5,7]. In such studies, CN is a signature of the chemical reaction between carbon and nitrogen. Thus, it is important in estimating the temperature of CN in a self-luminous high-temperature gas. However, the vibrational state of chemically reacting CN radicals is unlikely to have a Boltzmann distribution, as CN may be formed via chemical reactions during spectroscopic observations. This is because the characteristic time scale of the vibrational relaxation of CN ($\sim$1 μs) [8] is much longer than that of the radiation due to the electronic transition of the CN violet band system ($\sim$60 ns) [9]. A disturbed distribution of vibrational states affects the spectral shape, including the ratio of the intensities of the different band heads. As a result, we cannot estimate the temperature of chemically reacting nonequilibrium CN radicals based on a spectral-form-inversion analysis using the entire structure of their emission band. Failure to obtain the temperature of chemically reacting gas makes it is very difficult to understand the relevant reaction processes.

Both the translational and the rotational states reach a thermal equilibrium, as their relaxation time scales are very short [10,11]. The rotational state of chemically reacting CN should balance the translational state even if the vibrational state does not have a Boltzmann distribution, as explained in the following text. The characteristic time scale of equilibration between the rotational and translational states of N_2 is $\sim$20 ns at 10^4 K and 1 bar [11]. Because CN has a certain polarity, the characteristic time scale of equilibration between the rotational and translational states of CN is expected to be shorter than that of N_2. It is also expected to be shorter than that of the radiation due to the electronic transition of the CN violet band system. Thus, the rotational temperature is practically the same as the translational temperature. Therefore, we treat the two temperatures as a single temperature: the translational–rotational temperature. The translational temperature is also an important parameter in driving chemical reactions because it controls the collision probability of the gaseous particles in a chemically reacting hot gas. Thus, this study attempts to estimate the translational–rotational temperature of chemically reacting nonequilibrium CN radicals using emission spectroscopy.

Broadly speaking, three spectroscopic methods have been proposed in the literature for rotational-temperature measurements using molecular emission. The first involves plotting the logarithm of the intensities of the rotational lines normalized by the emission energy, transition probability, and statistical weight as a function of the rotational energy (i.e., a Boltzmann plot) [12]. The second method compares the shape of the band heads between the observed and theoretical synthetic spectra [13]. The third method measures the ratio of the irradiance of a bandhead and that of the depression between bandheads [14]. An advantage of these methods is their ability to estimate the rotational temperature directly.

A number of problems are inherent in the use of the preceding methods. In this study, we analyze emission spectra for which the vibrational states do not have a Boltzmann distribution. Thus, we should use the wavelength range that corresponds to only one electronic–vibrational transition when we use these three methods. Figure 1 illustrates the distribution of the rotational lines of the CN violet band system at 7000 K in thermal equilibrium, showing that the relevant wavelength range is 387.2–388.5 nm. This wavelength range corresponds to the (0,0) transition of the CN violet band system. The vibrational quantum numbers (v', v'') are indicated in the figure. Each sequence of points in the figure corresponds to an electronic–vibrational transition. The distribution pattern of a sequence is controlled only by the rotational temperature. The vibrational temperature controls the ratio of the emission intensities of the different sequences. The (0,0) bandhead is highly vulnerable to self-absorption in the CN violet band system. If self-absorption occurs (i.e., if the chemically reacting gas is optically thick), these methods cannot be applied directly to the emission spectra. In addition, the first method requires a very high spectral resolution to separate individual rotational lines within a band spectrum. The S/N ratio decreases as the spectral resolution increases for a given radiation source. The second and third methods also require a high spectral resolution because they use the bandhead structure in a narrow wavelength range. Thus, these methods are unsuitable when tracking temperature changes over a short period of time. Moreover, the second and third methods are affected by an additional uncertainty: the shape of the bandhead may have been altered by spectral line broadening of the rotational lines.

In this study, we focus on the blue ranges (CN: 379–381.5 nm, C_2: 490–502 nm) of the band systems of CN and C_2. Figure 1 shows that the range of wavelengths is largely controlled by emission lines of the R branch. The series of emission lines by a transition from J' to J'' are P and R branches (P branch: $J' - J'' = -1$, R branch: $J' - J'' = +1$). We call this fraction of the wavelength range the "band tail." We propose a new rotational-temperature-measurement method based on chemically reacting CN radicals using the band tails of their emission spectra. We call the new method the "band-tail fitting method." The effect of self-absorption in the band tail tends to be small because the optical thickness of the band tail is much smaller than that of the band heads, where many rotational lines overlap. In

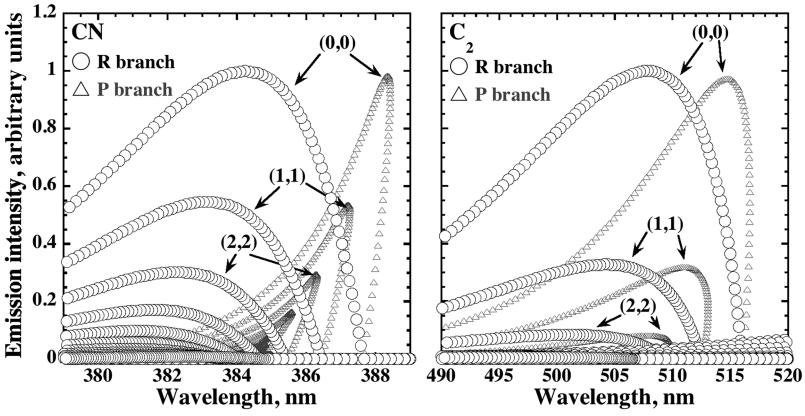

Fig. 1 Distribution of rotational lines in the CN violet band and C_2 Swan band systems.

addition, the band-tail fitting method can use much lower-resolution spectra than the other methods discussed previously, as it uses the spectral outlines of a band tail. Thus, our method is more suitable than previously developed methods for high-speed measurements (which are unable to obtain a large amount of light) of the temperature changes of chemically reacting CN radicals.

II. Band-Tail Analysis

In this section, we discuss the band-tail fitting method in detail. This section consists of three parts. We discuss the calculation procedure of the theoretical synthetic spectra in Sec. II.A, the effect of temperature on the spectral outline of the band tail in Sec. II.B, and the method of T_{rot} estimation using observed and theoretical spectra in Sec. II.C.

A. Calculation Procedure of Theoretical Synthetic Spectra

We use the CN violet band system ($B^2\Sigma^+ - X^2\Sigma^+$, $\Delta\nu = 0$) in this study. The C_2 Swan band system ($d^3\Pi_g - a^3\Pi_u$, $\Delta\nu = 0$) is also used to compare T_{rot} obtained for CN. Three steps are required to obtain a theoretical synthetic spectrum. In this calculation, we employ a widely used two-temperature model [15]. The first step is to calculate the emission and absorption coefficients as a function of wavelength for a given T_{rot} and T_{vib}. The second step is to calculate the radiative transfer in a radiative medium. The resulting spectrum is often called a "true spectrum." We assume that the radiation medium is optically thin, except in Sec. V.B. The computer software package SPRADIAN (structured package for radiation analysis) [16] was used to calculate the true spectra. In this band-emission calculation, SPRADIAN uses the Born–Oppenheimer approximation and the Franck–Condon principle; it calculates the diatomic potential energy on the basis of the Rydberg–Klein–Rees method. The line profile is assumed to be due to both Doppler and pressure broadening. The third step assesses the effect of the finite spectral resolution of spectrometers, to facilitate direct comparison with an observed spectrum. A synthetic spectrum I_{syn} is given by a convolution of a true spectrum and the instrumental spectrograph function Ψ [nm^{-1}]:

$$I_{syn}(\lambda) = \int I_{true}(\lambda + \Delta\lambda)\Psi(\Delta\lambda)\mathrm{d}\Delta\lambda \ [\mathrm{W\,m^{-2}\,nm^{-1}\,sr^{-1}}] \quad (1)$$

The instrumental function was obtained using the line profile of an emission line from an Hg lamp (ELECTRO-TECHNIC, Inc., Model SP200).

B. Effects of Rotational and Vibrational Temperatures on Spectral Shape

The band tail consists of many electronic–vibrational transitions (see Fig. 1). Thus, we must assess the effect of T_{rot} and T_{vib} on the spectral outline of the band tails of both CN and C_2. Figure 2 shows theoretical synthetic spectra for several values of T_{rot} and T_{vib}. Note that the spectral irradiance of the band tails of the theoretical synthetic spectra is normalized to maintain constant irradiance integrated over the entire wavelength range covered by the band tails (379–381.5 nm for CN, 490–502 nm for C_2). This figure clearly shows that the spectral outlines of the band tails of both CN and C_2 are solely controlled by T_{rot}. Thus, the band tails of CN and C_2 are expected to be good indicators of T_{rot}. Therefore, we can estimate T_{rot} using only the band tail in the spectral-form-inversion analysis.

C. Procedure of the Translational–Rotational-Temperature Estimation

The comparison between the observed and theoretical synthetic spectra proceeds as follows. We used two spectrograph gratings to obtain emission spectra, with groove densities of 150 lines mm^{-1} for C_2 and 2400 lines mm^{-1} for CN, to obtain the necessary wavelength resolution and coverage. For the grating with a groove density of 2400 lines mm^{-1} the spectral resolution [full width at half maximum (FWHM) $\sim$0.03 nm] is too high; it is very difficult to reproduce the fine structure of the band system, such as the exact wavelength of each rotational line, using this setup. Thus, we convolved the spectrum with a Gaussian kernel (FWHM = 0.1 nm) to reduce the effective spectral resolution of both the observed and theoretical synthetic spectra. Next, we carried out a spectral-form-inversion analysis using only the band tails of the emission spectra. The degree

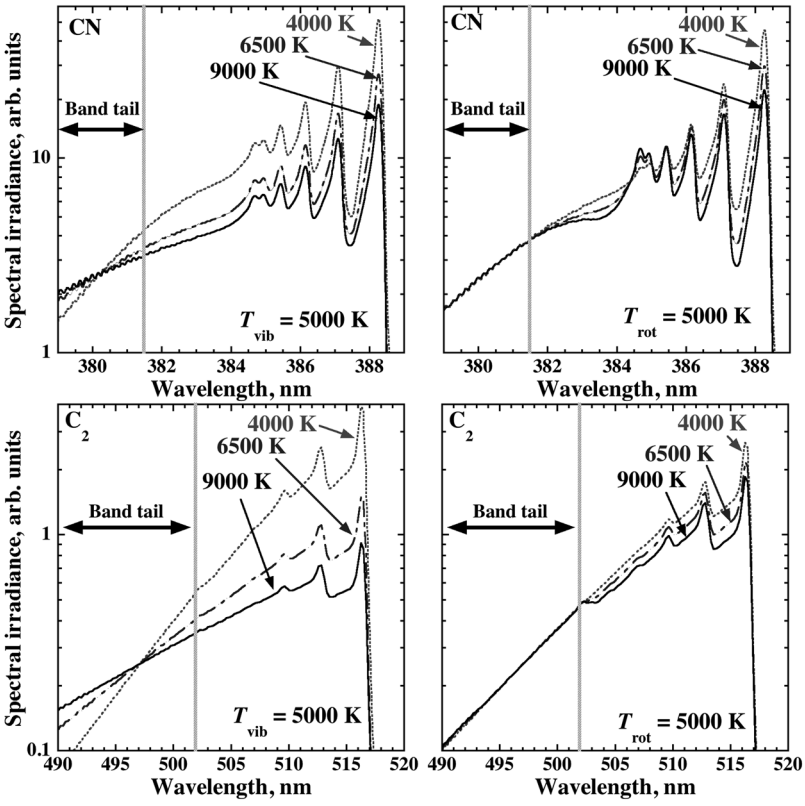

Fig. 2 Effect of T_{rot} (left) and T_{vib} (right) on the spectral shape of the band tails.

of difference is assessed on the basis of the quantity Er, defined as follows:

$$Er = \frac{\int [I_{\text{syn}}(\lambda) - I_{\text{obs}}(\lambda)]^2 \mathrm{d}\lambda}{\int [I_{\text{obs}}(\lambda)]^2 \mathrm{d}\lambda} \tag{2}$$

The parameter set that minimizes Er is considered the MLE of T_{rot} of the observed CN and C_2.

III. Laser-Ablation Experiments

Laser-ablation experiments are conducted within an $N_2 - H_2O - CO_2 - Ar$ atmosphere using graphite targets to investigate the validity of the band-tail fitting method. We discuss the experimental system in Sec. III.A, the experimental procedure in Sec. III.B, and the experimental conditions in Sec. III.C.

A. Experimental System

Laser-ablation experiments within N_2 gas using graphite targets are often conducted to investigate the production process of carbon-nitride thin films [3,17,18]. In the laser-induced carbon plume, C_2 radicals are produced due to atomic recombination of carbon atoms and ions or fragmentation of higher carbon clusters [17]. Then, CN radicals are produced by a gas phase reaction between the C_2 radicals and the ambient N_2 molecules near the boundary between a laser-induced carbon plume and the ambient gas [17]. We used band-emission spectra from these CN and C_2 radicals to investigate the validity of the band-tail fitting method.

Our experimental system consists of four components: an Nd: YAG laser, a vacuum chamber, gas cylinders, and an optical spectrometer (Fig. 3).

The laser wavelength is 1064 nm and the pulse width $\sim$13 ns. The irradiation frequency of the laser pulse is fixed at 1.0 Hz. The volume of the vacuum chamber is 8.9×10^2 ml. The vacuum chamber has four gas inlets to introduce a variety of gases independently. A manometer is used to control the mixing ratio of the gases. During the experiments the temperature of the wall of the vacuum chamber was kept at 80°C to prevent water condensation.

In this study, N_2, CO_2, Ar, and water vapor were used. Because we focused on chemically reacting CN radicals, we added CO_2 and H_2O gases. Laser-induced hot CN radicals are expected to react actively with the ambient CO_2 and H_2O gases. The presence of CO_2 and H_2O is important when applications to the atmospheric entry of probe vehicles [6], and meteoritic impacts on Earth [5,7] are considered. A small tank was filled with pure liquid water and connected to the chamber to introduce water vapor up to the saturated vapor pressure of approximately 30 mbar at room temperature.

The optical spectrometer consists of a spectrograph (Acton, SpectraPro 2750) and an intensified charge-coupled-device (ICCD) camera (Roper Scientific, PI–MAX). The focal length of the spectrograph is 750 mm. Wavelength resolutions and coverage are about 0.6 nm and 0.03 nm (FWHM) and 200 nm and 10 nm for the gratings with groove densities of 150 and 2400 lines mm^{-1}, respectively. The charge-coupled-device pixel-array size of the ICCD camera is 1024. A photodiode was used to trigger each spectroscopic observation. The delay time of this trigger system is about 0.2 μs. We obtained emission light from the entire laser-induced high-temperature vapor using a focusing lens installed in front of an optical fiber. The field of view (FOV) is $\sim$20 mm in diameter. The terminal radius of the laser-induced vapor cloud is constrained by the following relation:

$$P_{\text{atmos}} V_{\text{terminal}} \leq E_{\text{laser}} \tag{3}$$

$$V_{\text{terminal}} = \frac{2}{3} \pi r_{\text{terminal}}^3 \tag{4}$$

where P_{atmos}, V_{terminal}, E_{laser}, and r_{terminal} are the total pressure in the chamber ($=1.1 \times 10^3$ mbar), the volume of the vapor plume, the energy of the laser pulse ($=3.8 \times 10^2$ mJ), and the terminal radius of laser-induced carbon vapor, respectively. We assume that the shape of the laser-induced carbon plume is a hemisphere. The terminal radius of laser-induced carbon plume is 12 mm under the experimental condition. This value is significantly overestimated because we assume that the energy of the laser pulse is completely used as the work done against the ambient gas mixture by the carbon plume through its expansion. Thus, a laser-induced high-temperature vapor is expected to stay within the FOV during the spectroscopic observations. Hence, the T_{rot} obtained in this study is likely to represent an irradiance-weighted average value of T_{rot} in an entire laser-induced high-temperature vapor. We conducted calibration experiments for both wavelength and irradiance. Wavelength calibration for each grating was carried out using emission lines of the Hg lamp. A quartz–tungsten–halogen standard light source (Oriel Corporation, Model 63355) was used for irradiance calibration. Because the standard light source was too large to insert into the chamber, irradiance calibration was carried out outside the vacuum chamber; however, the same glass view port used in the laser experiments was placed between the standard lamp and the optical fiber to obtain calibration data including the effect of window absorption. Thus, we use a relative irradiance scale in this study.

B. Experimental Procedure

After a graphite target was placed on a stage, the vacuum chamber was evacuated to a residual pressure of $\sim 5.0 \times 10^{-4}$ mbar before

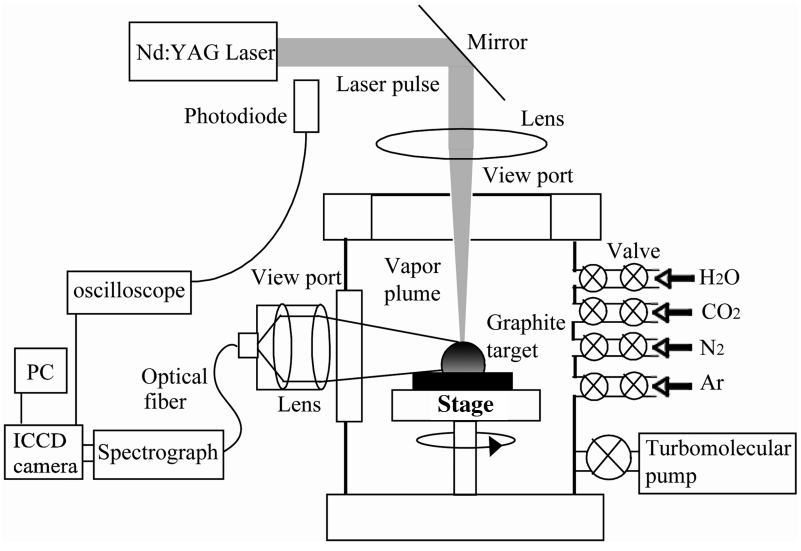

Fig. 3 Schematic configuration of the experimental system.

each experimental run. Water vapor, CO_2, N_2, and Ar were introduced into the vacuum chamber after evacuating the air. Subsequently, we started the laser irradiation and spectroscopic observation of the laser-induced CN and C_2 radicals. To increase the S/N ratio, 30 spectra measured under the same conditions were stacked. During the experiment, the target was rotated so as to irradiate the laser beam on a fresh surface of the target.

C. Experimental Conditions

We carried out two series of experiments in this study. First, we investigated the time evolution of T_{rot} of the laser-induced CN and C_2. The laser-beam diameter and intensity were fixed at 2.0 mm and 9.0×10^8 W cm^{-2}, respectively. The T_{rot} of the laser-induced CN and C_2 should decrease with time due to cooling processes, such as adiabatic expansion, radiation, and mixing with the cool ambient atmosphere.

Second, we investigated the dependence of the beam cross section on T_{rot}. The initial T_{rot} should be constant because the available laser energy per unit mass of vaporized carbon is the same at fixed beam intensity. The laser intensity was fixed at 5.0×10^8 W cm^{-2}, whereas the laser-beam diameter was varied from 1.3 to 2.7 mm. The exposure time was fixed at 0.2–10.2 μs after laser irradiation.

In all experiments the total pressure in the chamber was fixed at 1.1×10^3 mbar. The partial pressures of N_2, CO_2, H_2O, and Ar were 5.0×10^2, 2.6×10^2, 30, and 2.6×10^2 mbar, respectively.

IV. Experimental Results

This section first describes the results of the spectral comparison between the observed and theoretical synthetic spectra and the spectral-form-inversion analysis using the band tail of an observed spectrum. We then consider T_{rot} obtained as a function of time and beam cross section.

A. Emission Spectra

We obtained low- and high-wavelength-resolution emission spectra using two gratings, as discussed in Sec. III.A. Figure 4 shows the time evolution of the low-wavelength-resolution (FWHM ~0.6 nm) spectra. The exposure times after laser irradiation are indicated in the figure. The main emission sources were CN and C_2. A strong blackbody continuum was observed immediately after laser irradiation. We use these spectra to estimate the rotational temperature of C_2. Here, it is noted that there is a strong N_2^+ band emission (first negative system) in the observed wavelength range. If the N_2^+ first negative band is strong, we cannot apply the band-tail fitting method directly because the N_2^+ first negative system overlaps the CN violet band system [19]. However, a significant emission from the band was not observed in our experiments. Thus, the effect of the N_2^+ band does not have to be considered in the analysis in this study.

Figure 5 shows the observed high-wavelength-resolution spectra obtained under the same conditions as in Fig. 4. Note that the background continuum has been subtracted. The exposure times after laser irradiation and the vibrational quantum numbers (ν', ν'') are indicated in Fig. 5. The intensity of the (1,1) bandhead is nearly equal to that of its (0,0) equivalent in the spectra shown in panels b and c. Because the transition probability of the (1,1) transition is 1.2 times smaller than that of (0,0) [9] the vibrational temperatures of these spectra would be negative if we assumed that the vibrational states have a Boltzmann distribution. Thus, laser-induced CN radicals are clearly out of equilibrium under our experimental conditions. Panel e shows a close-up of the (0,0) bandhead immediately after laser irradiation and a theoretical synthetic spectrum for the optimum T_{rot} estimated in Sec. IV.B. The (0,0) bandhead of the observed spectrum immediately after laser irradiation may be affected by self-absorption because its cusp is blunt. Panel e also shows that the wavelength resolution is too low to produce a Boltzmann plot for the rotational lines.

Figure 6 shows a relevant comparison between an observed CN spectrum and three theoretical synthetic spectra for different temperatures. The thick line shows the observed spectrum obtained from 2.2 to 4.2 μs after laser irradiation. Panels c and d show the residuals of the band tails between the observed spectrum and the three theoretical synthetic spectra of panels a and b, respectively. Note that the three residual lines for panel d mostly overlap. If T_{rot} of the theoretical synthetic spectra is fixed at the optimum value, the band tails of both the observed and theoretical synthetic spectra are in good agreement, regardless of the value of T_{vib}. In contrast, significant differences are seen if we vary T_{rot}.

Figure 7 shows a contour map of Er as a function of both T_{rot} and T_{vib}. The observed spectra of CN and C_2 used for these calculations are obtained 2.2–4.2 μs after laser irradiation. This figure shows that Er strongly depends on T_{rot}. In contrast, Er is nearly constant for T_{vib}. This clearly indicates that the band-tail fitting method can determine T_{rot}.

B. Temperatures for Each Experimental Condition

In this section, we discuss T_{rot} obtained using the band-tail fitting method as a function of both time and beam cross section.

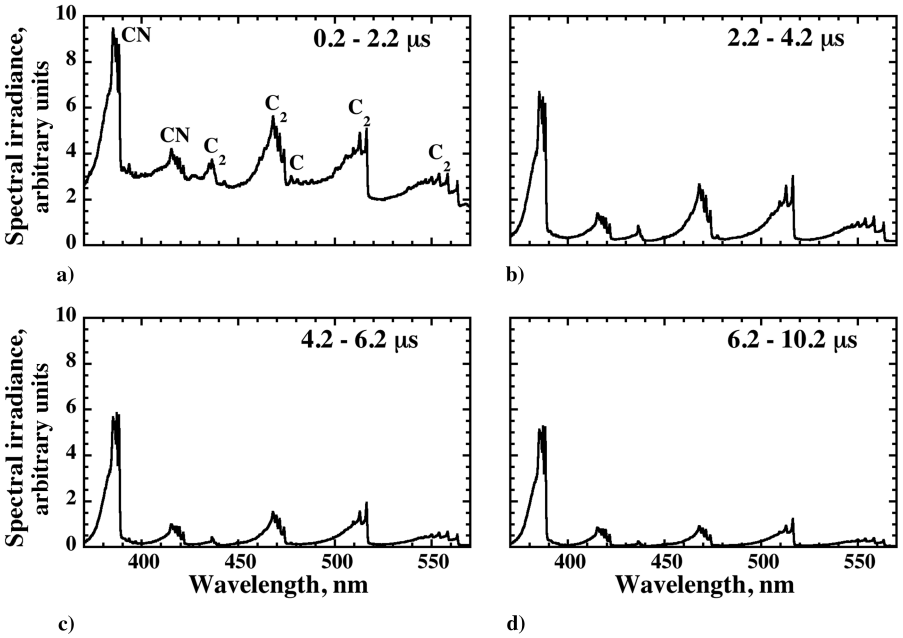

Fig. 4 Low-wavelength-resolution observed emission spectra of laser-induced vapor clouds.

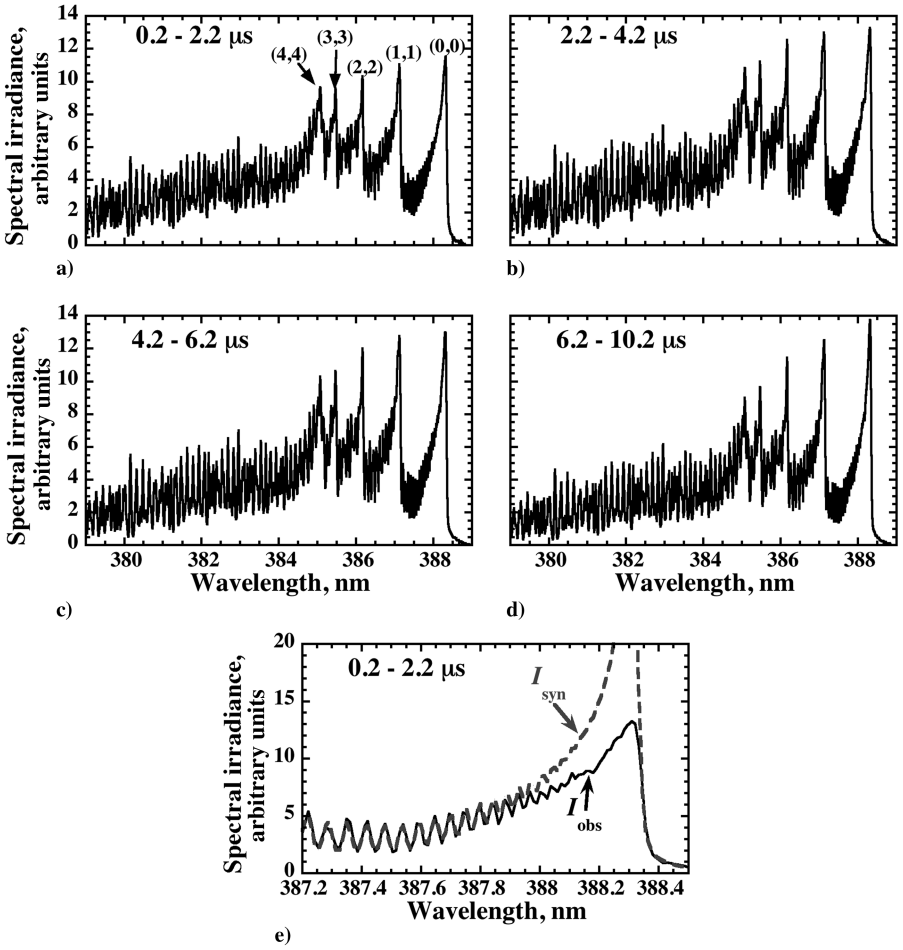

Fig. 5 High-wavelength-resolution observed emission spectra of laser-induced vapor clouds.

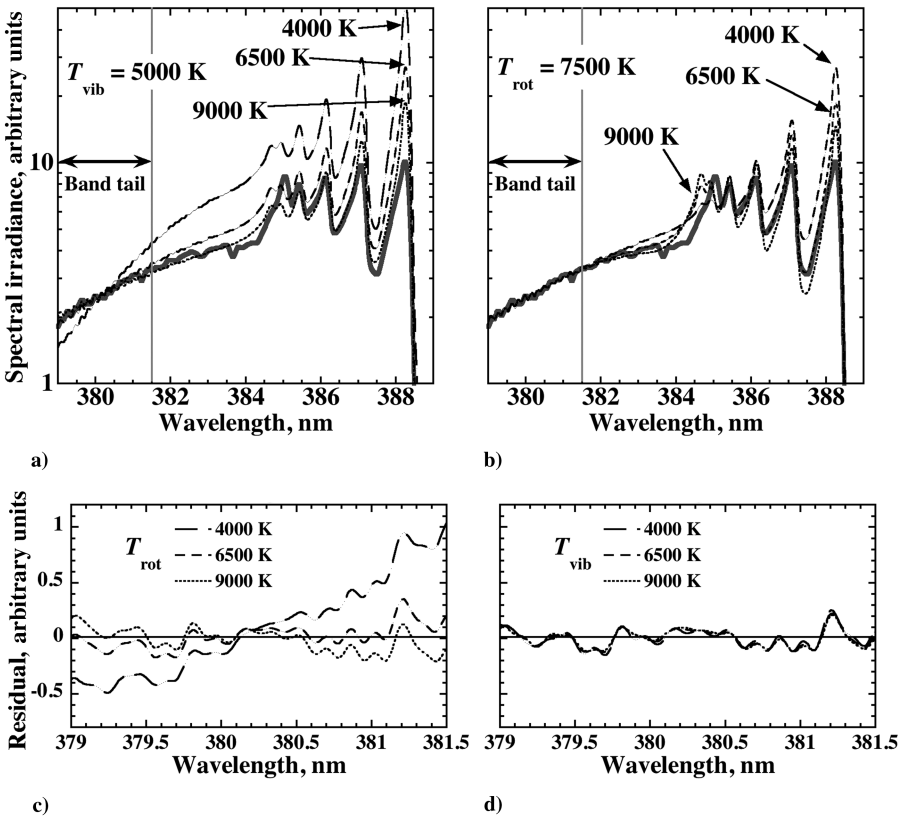

Fig. 6 Comparison of an observed CN spectrum (solid gray line) with three theoretical synthetic spectra for different temperatures.

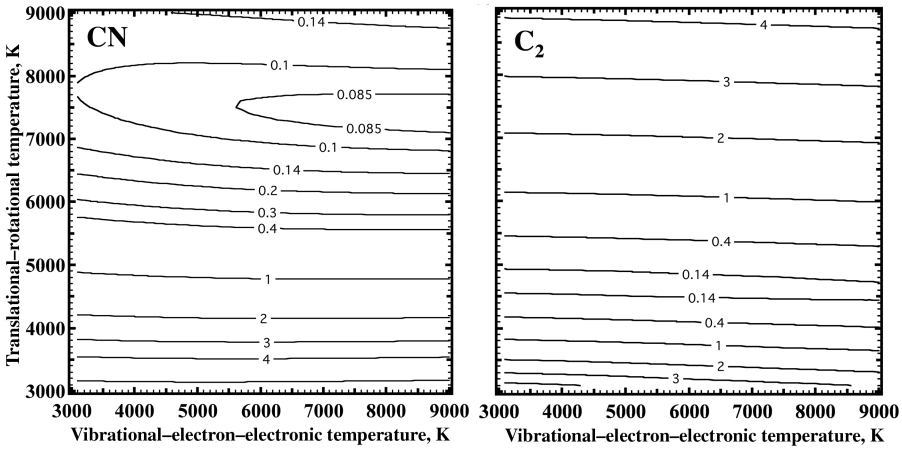

Fig. 7 Contour maps of *Er* (%) as a function of both T_{rot} and T_{vib} for CN and C_2.

Figure 8 shows T_{rot} values of the laser-induced CN and C_2 radicals as a function of time. Two data points were obtained for each exposure time. Horizontal and vertical bars represent the exposure times and fitting errors due to random noise in observed spectra in T_{rot}, respectively. Because T_{rot} is estimated from minimization of Er, we need to use a rather involved method to estimate the fitting errors. We used a Monte Carlo method called the bootstrap method [20] to investigate fitting errors due to random noise in observed spectra. The procedure to estimate the fitting errors is as follows. First, a half of the data points are excluded from an observed band-tail spectrum randomly. Then, we conduct the band-tail fitting analysis with the partial data set. This calculation is repeated 250 times with different random choices of data exclusion. The distribution of T_{rot} estimated from the partial data sets is similar to a Gaussian distribution. The standard deviation of obtained T_{rot} is expected to give fitting errors due to random noise in the observed spectra. The estimated fitting errors range from 2 to 4%. The reproducibility errors derived from the variation between different shots repeated under the same experimental condition are on the same order of magnitude (2–7%) as the fitting errors. The temperatures of both CN and C_2 decrease with time in a similar fashion; however, the rotational temperature of CN is significantly higher than that of C_2. This result is consistent with previous similar laser-ablation experimental studies [3,17,18] under much thinner atmospheric conditions (with a partial pressure of N_2 of about 0.01–10 mbar). The rotational temperature of CN is higher than that of C_2 because the kinetic energy of C_2 is converted into the thermal energy of CN via energetic collisions between C_2 and N_2.

Figure 9 shows the T_{rot} of the laser-induced CN and C_2 radicals as a function of beam cross section. Five data points were obtained for each beam cross section. The initial T_{rot} of the laser-induced CN is nearly constant for different beam cross sections when the laser-beam intensity is fixed. The reason for this trend is discussed in Sec. III.C.

These results show that the band-tail fitting method can reproduce the physically predicted trends of T_{rot} as a function of both time evolution and beam cross section.

V. Discussion

This section consists of three parts. We discuss the error evaluation of the band-tail fitting method in Sec. V.A, the effects of variable wavelength resolution and optical thickness on the spectral outlines of the band tails in Sec. V.B, and compare the band-tail fitting method with conventional spectral-form-inversion analysis in Sec. V.C.

A. Error Evaluation of the Band-Tail Fitting Method

The spectroscopic constants used in SPRADIAN have an associated uncertainty, leading to a systematic error in the estimation of T_{rot}. Thus, we should estimate the range of MLEs of the temperature based on the uncertainty in the spectroscopic constants.

As discussed in Sec. II.B, the band tails of the emission spectra of the CN violet band and the C_2 Swan band system are controlled by T_{rot}. Thus, the spectroscopic constants of the vibrational term such as $\omega_e x_e$, $\omega_e y_e$, and $\omega_e z_e$ are not relevant for rotational-temperature estimation using the band-tail fitting method.

The most influential spectroscopic constant of the band-tail fitting method is a rotational constant B_e [cf. Eqs. (8) and (9)]. The reason for this is as follows. The emission intensity of each rotational line is given by [21]

$$I_{v''J''}^{v'J'} = \frac{1}{4\pi}\frac{hc}{\lambda_{v''J''}^{v'J'}} A_{v''J''}^{v'J'} N_{v'J'} \tag{5}$$

where I is the emission intensity. The transition probability of CN can be separated into vibrational and rotational terms using

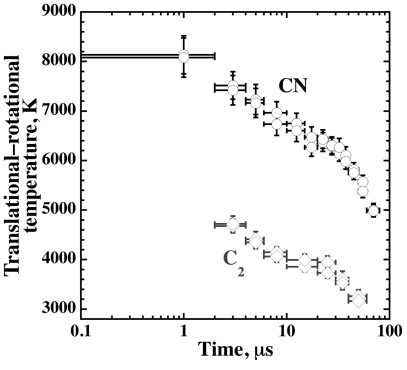

Fig. 8 T_{rot} of laser-induced CN and C_2 radicals as a function of time.

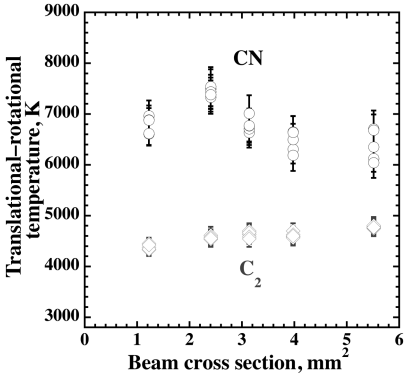

Fig. 9 T_{rot} of laser-induced CN and C_2 radicals as a function of beam cross section.

$$A_{v''J''}^{v'J'} = \left(\frac{\lambda_{v'v''}}{\lambda_{v''J''}^{v'J'}}\right)^3 \frac{A_{v'v''}S_{J'J''}}{(2J'+1)} \tag{6}$$

where $\lambda_{v'v''}$, $A_{v'v''}$, and $S_{J'J''}$ are the wavelength of the band origin, the transition probability of the electronic–vibrational transition, and the Hönl–London factor, respectively [16]. Assuming that the rotational state of CN is in thermal equilibrium, the rotational term of the emission intensity is described by

$$I_{v''J''}^{v'J'} \propto \left(\frac{1}{\lambda_{v''J''}^{v'J'}}\right)^4 S_{J'J''} \exp\left(-\frac{F(J')}{kT_{\text{rot}}}\right) \tag{7}$$

The rotational energy and the wavelength of the rotational line are given by

$$F(J') = B_{v'}J'(J'+1) - D_{v'}J'^2(J'+1)^2 \tag{8}$$

$$B_{v'} = B_e - \alpha_e\left(v' + \frac{1}{2}\right), \qquad D_{v'} = D_e + \beta_e\left(v' + \frac{1}{2}\right) \tag{9}$$

and

$$\lambda_{v''J''}^{v'J'} = \left(\frac{1}{\lambda_{v'v''}} + F(J') - F(J'')\right)^{-1} \tag{10}$$

where B_e, α_e,D_e, and β_e are spectroscopic constants. The rotational quantum numbers corresponding to the wavelengths of the CN band-tail range from 55 to 68 for the (0,0) transition. In this case, the first term of Eq. (8) is ~100 times the second term, and B_e is ~90 times α_e [21]. Thus, the rotational energy $F(J')$ is practically equal to $B_eJ'(J'+1)$. Consequently, B_e is the dominant spectroscopic constant controlling the estimated temperature in the band-tail fitting method. Because the first term of the wavelength of each rotational line is ~50 times the second term, the uncertainty in the wavelength of each rotational line due to B_e is negligible. Also, the uncertainty in $\lambda_{v'v''}$ does not change the spectral outline of the band tail, because $\lambda_{v'v''}$ does not depend on J. Thus, the largest uncertainty in the emission intensity due to the uncertainty in B_e is the Boltzmann factor of the rotational term $\exp(-B_eJ'(J'+1)/kT_{\text{rot}})$. Consequently, the systematic error in T_{rot} is of the same order of magnitude as that of B_e. A number of researchers have estimated B_e [21–23]. The difference in B_e estimated in these studies is less than 1%. Consequently, the systematic error in T_{rot} estimated in this study is also less than 1%. Thus, the observed temperature difference between CN and C_2, ~2000 K (i.e., >25% of the CN and C_2 temperatures), is most likely real. This result supports the conclusion that our method is robust with respect to the uncertainties in the spectroscopic constants.

B. Effects of Wavelength Resolution and Optical Thickness

In this section, we discuss the effects of wavelength resolution and optical thickness on temperature estimation using the band-tail fitting method. In this study, we convolved a Gaussian kernel with the observed and theoretical synthetic spectra, as discussed in Sec. II.C. We conducted a spectral-form-inversion analysis using the band tail of the emission spectra convolved with different Gaussian FWHM values to investigate the effect of wavelength resolution. Figure 10 shows the theoretical synthetic spectra and Er as a function of T_{rot} for three values of FWHM. The left-hand panel shows that the spectral shapes of the band tails are unaffected by the Gaussian FWHM adopted. The band tails of the three spectra are in good agreement and the optimum T_{rot} is nearly constant, regardless of FWHM. These results strongly suggest that the band-tail fitting method requires much lower-wavelength-resolution spectra than other rotational-temperature-measurement methods. Note that this result also shows that the MLE of the temperature is unaffected by the smoothing method.

To investigate the effects of optical thickness, we calculate theoretical synthetic spectra for several values of the column number density of the CN radicals. The result is shown in Fig. 11; the effects of the optical thickness on the band tail and the bandhead of the (0,0) transition are shown in the left- and right-hand panels, respectively. The column number densities of CN are shown in the figure. Blackbody radiation at the same temperature is also shown in the left-hand panel of the figure. Note that the spectral irradiance of the band tail (left) and the bandhead (right) of the theoretical synthetic spectra have been normalized to maintain constant irradiance integrated over the entire wavelength range (379–381.5 nm for the band tail, 387.5–388.5 nm for the bandhead). As the column number density of CN increases, the emission spectrum approaches gradually Planck function. The slope of Planck function in the wavelength range of the band tail of CN is much more gentle than that of the band-tail spectra of CN for typical temperature (5000–10,000 K) in this study (see the left-hand panel of the Fig. 11). Thus, self-absorption causes a systematic overestimation of T_{rot} in the band-tail fitting method when we used optically thin theoretical synthetic spectra. The band tail is free from self-absorption if the column number density of CN is less than ~20 nmol cm^{-2}. In contrast, the spectral shape of the bandhead is highly vulnerable to self-absorption. In our actual experiments, it is difficult to estimate the column number density of laser-induced nonequilibrium CN radicals because the electronic state of CN is also expected to be out of an equilibrium population. The degree of self-absorption is controlled by the population of both upper and lower electronic states. Thus, we cannot estimate the systematic error due to self-absorption in observed T_{rot} quantitatively. Nevertheless, in Fig. 11, we demonstrate that the spectral shape of band tail is much more robust against self-absorption than the bandhead under the same radiation environment.

C. Comparison with Conventional Spectral-Form-Inversion Analysis

Because the irradiance of the CN band tail is smaller than that of the bandhead, the influence of the band tail on the spectral-form-inversion analysis is smaller than that of the bandhead. As discussed in Sec. II.B, the band tails of the emission spectra of the CN violet

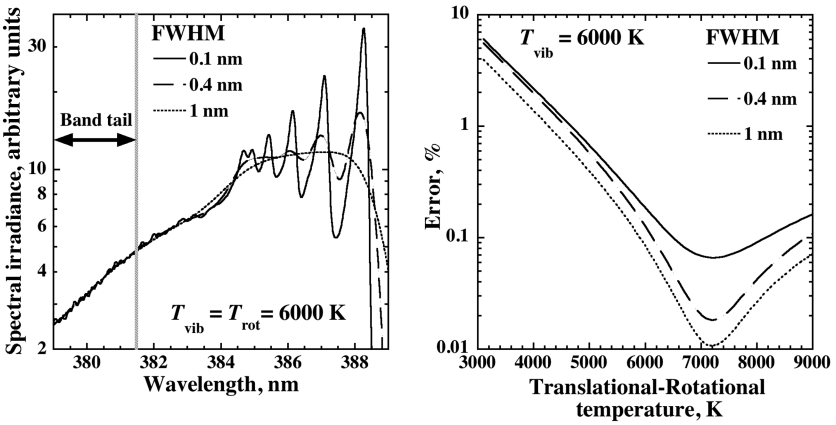

Fig. 10 Theoretical synthetic spectra and Er as a function of T_{rot} for three values of the Gaussian FWHM.

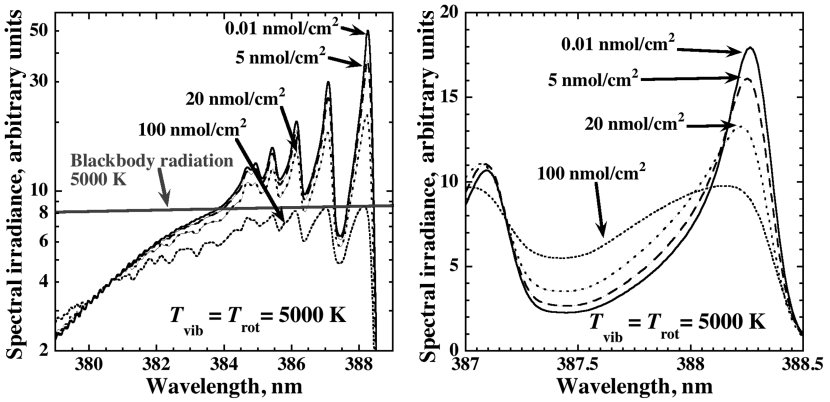

Fig. 11 Effect of CN column number density on the band tail (left) and bandhead (right) of the (0,0) transition.

band and the C_2 Swan band systems are controlled only by T_{rot}. Also, as discussed in Secs. V.A and V.B, the shape of the band tail is highly insensitive to the uncertainties in the spectroscopic constants and to self-absorption. In contrast, the bandhead is likely to deviate from the equilibrium shape of the band system due to the nonequilibrium distribution of the vibrational state and self-absorption. Thus, if a spectral-form-inversion analysis using the entire structure of a band system fails to fit the band tail, an optimum T_{rot} that minimizes Er may not be as good a measure for the rotational temperature. In such a case, the band-tail fitting method proposed in this study would give a more accurate estimate of the rotational temperature.

VI. Conclusions

We developed a new rotational-temperature-measurement method for chemically reacting nonequilibrium CN radicals using the band tails of the emission spectra. The results of this study show that the band tails of the emission spectra of CN and C_2 are controlled only by the rotational temperature. Thus, the band tails can serve as a good indicator of the rotational temperature. The band-tail fitting method has two advantages: it is insensitive to self-absorption and can use much lower-resolution spectra than other rotational-temperature-measurement methods.

Laser-ablation experiments within $N_2 - H_2O - CO_2 - Ar$ atmospheres using graphite targets were conducted to investigate the validity of our method. We observed laser-induced nonequilibrium CN radicals and estimated the translational–rotational temperature. Experimental results show that the rotational temperatures obtained can reproduce the physically predicted trends as a function of time and beam cross section. The systematic error due to uncertainties in the spectroscopic constants in the band-tail fitting method is of the same order as the uncertainty in the spectroscopic constants. These results strongly suggest that our method can serve as a powerful tool in measuring the translational–rotational temperature of chemically reacting nonequilibrium CN radicals.

Acknowledgments

This research was partially supported by a grant-in-aid from Japan Society for the Promotion of Science. Kosuke Kurosawa thanks Y. Takama of the University of Tokyo for discussions on spectroscopic analysis. Kosuke Kurosawa also thanks K. Watanabe and M. Okada of the University of Tokyo for discussions on error evaluation. We thank two anonymous reviewers and D. Levin as editor for providing helpful comments and suggestions.

References

[1] Griem, H. R., *Plasma Spectroscopy*, McGraw–Hill, New York, 1964.

[2] Arnold, J. O., Whiting, E. E., and Lyle, G. C., "Line by Line Calculation of Spectra from Diatomic Molecules and Atoms Assuming a Voigt Line Profile," *Journal of Quantitative Spectroscopy and Radiative Transfer*, Vol. 9, No. 6, 1969, pp. 775–798. doi:10.1016/0022-4073(69)90075-2

[3] Vivien, C., Hermann, J., Perrone, A., Boulmer–Laborgne, C., and Luches, A., "A Study of Molecule Formation During Laser Ablation of Graphite in Low-Pressure Nitrogen," *Journal of Physics D: Applied Physics*, Vol. 31, No. 10, 1998, pp. 1263–1272. doi:10.1088/0022-3727/31/10/019

[4] Fujita, K., Sato, S., Abe, T., and Ebinuma, Y., "Experimental Investigation of Air Radiation from Behind a Strong Shock Wave," *Journal of Thermophysics and Heat Transfer*, Vol. 16, No. 1, 2002, pp. 77–82. doi:10.2514/2.6654

[5] Sugita, S., and Schultz, P. H., "Interactions Between Impact-Induced Vapor Clouds and the Ambient Atmosphere: 1. Spectroscopic Observations Using Diatomic Molecular Emission," *Journal of Geophysical Research*, Vol. 108, No. E6, 2003, p. 5051. doi:10.1029/2002JE001959

[6] Rond, C., Boubert, P., Fèlio, J.-M., and Chikhaoui, A., "Nonequilibrium Radiation Behind a Strong Shock Wave in $CO_2 - N_2$," *Chemical Physics*, Vol. 340, Nos. 1–3, 2007, pp. 93–104. doi:10.1016/j.chemphys.2007.08.003

[7] Sugita, S., and Schultz, P. H., "Interactions Between Impact-Induced Vapor Clouds and the Ambient Atmosphere: 2. Theoretical Modeling," *Journal of Geophysical Research*, Vol. 108, No. E6, 2003, p. 5052. doi:10.1029/2002JE001960

[8] Slack, M. W., "Kinetics and Thermodynamics of the CN Molecule. III. Shock Tube Measurement of CN Dissociation Rates," *Journal of Chemical Physics*, Vol. 64, No. 1, 1976, pp. 228–236. doi:10.1063/1.431955

[9] Knowles, P. J., Werner, H.–J., Hay, P. J., and Cartwright, D. C., "The $A^2\Pi - X^2\Sigma^+$ Red and $B^2\Sigma^+ - X^2\Sigma^+$ Violet Systems of the CN Radical: Accurate Multireference Configuration Interaction Calculations of the Radiative Transition Probabilities," *Journal of Chemical Physics*, Vol. 89, No. 12, 1988, p. 7334. doi:10.1063/1.455264

[10] Zel'dovich, Y. B., and Raizer, Y. P., *Physics of Shock Waves and High-Temperature Hydrodynamic Phenomena*, Dover, New York, 1967.

[11] Fujita, K., "Assessment of Molecular Internal Relaxation and Dissociation by DSMC-QCT Analysis," *39th AIAA Thermophysics Conference*, AIAA Paper 2007-4345, 2007.

[12] Duten, X., Rousseau, A., Gicquel, A., and Leprince, P., "Rotational Temperature Measurements of Excited and Ground States of $C_2(d^3\Pi g - a^3\Pi u)$ Transition in a H_2/CH_4 915 MHz Microwave Pulsed Plasma," *Journal of Applied Physics*, Vol. 86, No. 9, 1999, pp. 5299–5301. doi:10.1063/1.371515

[13] Gomès, A. M., Barci, J., Sarrette, J. P., and Salon, J., "Measurement of Heavy Particle Temperature in a RF Air Discharge at Atmospheric Pressure from the Numerical Simulation of the $NO\gamma$ System," *Journal of Analytical. Atomic Spectroscopy*, Vol. 7, No. 7, 1992, pp. 1103–1109. doi:10.1039/ja9920701103

[14] Park, C. S., Newfield, M. E., Fletcher, D. G., Gökçen, T., and Sharma, S. P., "Spectroscopic Emission Measurements Within the Blunt-Body Shock Layer in an Arcjet Flow," *Journal of Thermophysics and Heat Transfer*, Vol. 12, No. 2, 1998, pp. 190–197. doi:10.2514/2.6344

[15] Park, C., "Assessment of Two-Temperature Kinetic Model for Ionizing Air," *Journal of Thermophysics and Heat Transfer*, Vol. 3, No. 3, 1989, pp. 233–244. doi:10.2514/3.28771

[16] Fujita, K., and Abe, T., "SPRADIAN, Structured Package for Radiation Analysis: Theory and Application," The Institute of Space and Astronautical Science, Rept. 669, Japan, 1997, pp. 1–47.

[17] Thareja, R. K., Dwivedi, R. K., and Ebihara, K., "Interactions of Ambient Nitrogen Gas and Laser Ablated Carbon Plume: Formation of CN," *Nuclear Instruments and Methods in Physics Research. Section B*, Vol. 192, No. 3, 2002, pp. 301–310. doi:10.1016/S0168-583X(02)00476-7

[18] Wee, S., and Park, S. M., "Reactive Laser Ablation of Graphite in a Nitrogen Atmosphere: Optical Emission Studies," *Optics Communications*, Vol. 165, Nos. 4–6, 1999, pp. 199–205. doi:10.1016/S0030-4018(99)00217-5

[19] Pearce, R. W. B., and Gaydon, A. G., *The Identification of Molecular Spectra*, 4th ed., CRC Press, Boca Raton, FL, 1976.

[20] Efron, B., and Tibshirani, R. J., *An Introduction to the Bootstrap*, CRC Press, Boca Raton, FL, 1993.

[21] Hertzberg, G., *Molecular Spectra and Molecular Structure, I, Diatomic Molecules*, 2nd ed., Krieger, Malabar, FL, 1950.

[22] Huber, K. P., and Hertzberg, G., *Molecular Spectra and Molecular Structure, IV. Constants of Diatomic Molecules*, Van Nostrand Reinhold, New York, 1979.

[23] Praced, C. V. V., and Bernath, P. F., "Fourier Transform Jet-Emission Spectroscopy of the $A^2\Pi_i - X^2\Sigma^+$ Transition of CN," *Journal of Molecular Spectroscopy*, Vol. 156, No. 2, 1992, pp. 327–340. doi:10.1016/0022-2852(92)90235-G